Biosensors and Bioelectronics 141 (2019) 111440

Contents lists available at ScienceDirect

Biosensors and Bioelectronics

journal homepage: www.elsevier.com/locate/bios

Analyte-resolved magnetoplasmonic nanocomposite to enhance SPR signals and dual recognition strategy for detection of BNP in serum samples

Jialin Zhao[a,b], Danli Liang[a], Shouwei Gao[c], Xiaojun Hu[a], Kwangnak Koh[d], Hongxia Chen[a,*]

[a] Center for Molecular Recognition selectivity and Biosensing, School of Life Sciences, Shanghai University, Shanghai, 200444, China
[b] Shanghai Key Laboratory of Bio-Energy Crop, School of Life Sciences, Shanghai University, Shanghai, 200444, China
[c] School of Mechatronic Engineering and Automation, Shanghai University, Shanghai, 200444, China
[d] Institute of General Education, Pusan National University, Busan, 609-735, Republic of Korea

ARTICLE INFO

Keywords:
Surface plasmon resonance
Nanocomposite
GNPs-apt
MNPs-ab
Serum sample

ABSTRACT

B-type natriuretic peptide (BNP) is a short peptide that is considered to be an important heart failure (HF)-related biomarker. Due to its low concentration in the blood and short half-life, the sensitive detection of BNP is a bottleneck for diagnosing patients at early stages of HF. In this paper, we report a facile surface plasmon resonance (SPR) sensor to measure BNP; the sensor is based on aptamer-functionalized Au nanoparticles (GNPs-Apt) and antibody-modified magnetoplasmonic nanoparticles (MNPs-Ab) to enable dual screening of BNP in complex environments. During sensing, BNP forms MNP-Ab/BNP/GNP-Apt nanoconjugates that can be rapidly separated from the complex sample by a magnet to avoid degradation within the analyte's half-life. The developed SPR biosensor shows high selectivity, a wide dynamic response range of BNP concentrations from 100 fg/mL to 10 ng/mL, and a low detection limit of 28.2 fg/mL (S/N = 3). Using the proposed sensor, BNP was successfully detected in clinical samples. Thus, the designed SPR biosensor provides a novel and sensitive sensing platform for BNP detection with potential applications in clinical practice.

1. Introduction

B-type natriuretic peptide (BNP) is a short peptide composed of 32 amino acids that is secreted by cardiomyocytes. It is used as a standard molecular biomarker to provide important physiological and pathological information for the diagnosis and prognosis of chronic heart failure (HF) (Lin et al., 2014; Li et al., 2019a,b; Liu et al., 2014; Goetze et al., 2016). Clinically, when 100 pg/mL BNP is used as a detection threshold, its potential prediction reaches 90%, which can reduce clinical uncertainty by 74%. A BNP level of over 400 pg/mL indicates a 95% possibility of HF (Rogers et al., 2014; Lourenço et al., 2009). BNP is more difficult to detect than other cardiovascular biomarkers because of its pictogram-level of content in biological samples and the complexity of these samples. The 22-min half-life of BNP presents another challenge. Several methods for BNP determination, including fluorescent immunoassays (Jang et al., 2014; Ahmed et al., 2014; Lei et al., 2017), colorimetric (Wang et al., 2014), quartz crystal microbalance immunoassays (Altintas et al., 2014), and electrochemical immunoassays (Serafín et al., 2018; Xu et al., 2018; Sarangadharan et al., 2018; Chekin et al., 2018), have been reported. Unfortunately, the accuracy and expiry date of these methods do not satisfy the requirements of quantitative and rapid determination (Lei et al., 2017; Li et al., 2019a,b). Therefore, a facile and sensitive device to measure BNP levels must be developed.

Surface plasmon resonance (SPR) is a leading technology that allows the sensitive and real-time detection of the interaction between ligands on chips and target biomolecules (Abbas et al., 2011; Jang et al., 2014; Scarano et al., 2010). Despite its many benefits, however, the SPR technique is limited by its low sensitivity, especially for small molecules (Li et al., 2015; Liang et al., 2014; Cao et al., 2018). To enhance the sensitivity of SPR, a number of nanomaterials with high refractive indices or optical properties (e.g., Au nanoparticles (GNPs), silver nanoparticles, and magnetoplasmonic nanoparticles (MNPs)) have been introduced to fabricate SPR biosensors (He et al., 2010; Liang et al., 2012; Wu et al., 2016; Jain et al., 2007; Wang et al., 2010). MNPs have drawn marked attention because of their unique optical and magnetic properties. MNPs are typically used as separation supports (Fathi et al., 2019; Feng et al., 2016; Babamiri et al., 2017; Liu et al., 2015; Li et al., 2016; Egesa et al., 2018). The combination of GNPs with a magnetic core can provide stable binding sites, separation properties, and signal enhancement in SPR. In our previous work (Mei et al., 2012; Chen et al., 2015; Zou et al., 2017), addition of spherical MNPs@GNPs-Ab

* Corresponding author.
E-mail address: hxchen@shu.edu.cn (H. Chen).

https://doi.org/10.1016/j.bios.2019.111440
Received 24 April 2019; Received in revised form 12 June 2019; Accepted 14 June 2019
Available online 19 June 2019
0956-5663/

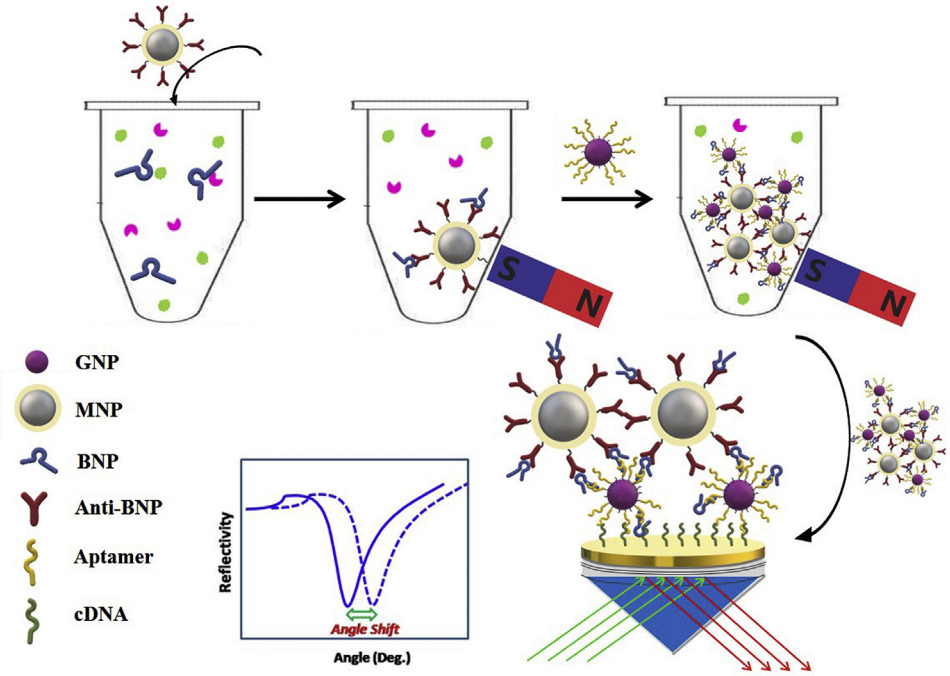

Scheme 1. Schematic of the BNP SPR sensing strategy via magnetoplasmonic nanocomposites for signal amplification.

conjugates resulted in a remarkable increase in SPR angles, thereby indicating that core–shell MNPs@GNPs can amplify the sensitivity of SPR sensors. However, core–shell MNPs@GNPs demonstrate easy aggregation, which means these particles adsorb onto the chip surface nonspecifically and could yield a positive false signal. To solve this problem, analyte-resolved MNPs are proposed to enhance SPR signals.

In this work, we designed a facile and sensitive SPR device to measure BNP; this sensor is based on aptamer-functionalized GNPs (GNPs-Apt) and antibody-modified MNPs (MNPs-Ab) to enable dual screening of BNP in complex environments. BNP forms MNPs-Ab/BNP/GNPs-Apt nanoconjugates that can be separated from complex samples by an external magnetic field to avoid degradation. The complementary-DNA (cDNA) of the aptamer immobilized on the Au film binds with MNPs-Ab/BNP/GNPs-Apt nanoconjugates in a facile manner through hybridization with the GNPs-Apt (Scheme 1). The analyte-resolved magnetoplasmonic nanoconjugates promote strong electric coupling between MNPs and the surface plasmon wave of GNPs and produces changes in the refractive index of the chip surface. Conjugate formation also leads to increases in mass change and contributes to the significant SPR signal enhancement of the BNP sensor. Furthermore, cDNA enables dual selective binding to eliminate nonspecific binding. A highly sensitive and selective format for BNP measurement is fabricated to meet the performance requirements of clinical application.

2. Experimental section

2.1. Reagents and apparatuses

Hydrogen tetrachloroaurate trihydrate ($HAuCl_4 \cdot 3H_2O$), Myoglobin (Mb), Ascorbic Acid (AA), ovalbumin (OVA), 11-mercaptoundecanoic acid (MUA), 1-ethyl-3-(3-dimethylaminopropyl) carbodiimide hydrochloride (EDC) and N-hydroxysulfosuccinimide (NHS) were purchased from Sigma–Aldrich (Shang Hai, China). Bovine hemoglobin (BHb), Bovine serum albumin (BSA) were obtained from Sinopharm Chemical Reagent Co., Ltd. (Shanghai, China), Fe_3O_4 nanoclusters were purchased from AMO Life Science Inc. (Amo-Mag, Kimpo, Korea). B-type natriuretic peptide (BNP) and antibody-BNP (anti-BNP) were purchased from Sangon Biotech Co., Ltd. (Shanghai, China). All aptamers were synthesized by Sangon Biotech Co., Ltd. (Shanghai, China). BNP-specific aptamer: 5′-H_2N-TTT TTT TAA ACG CTC AAA GGA CAG AGG GTG CGT AGG AAG GGT ATT CGA CAG GAG GCT CAC A-3′. Complementary sequence (cDNA): 5′-SH-TGT GAG CCT CCT GTC GAA TAC CCT TCC TAC GCA CCC TCT GTC CTT TGA GCG TTT AAA AAA A-3′. All solutions were treated with deionized water (DW) and purified using a Milli-Q distillation system (Branstead, USA) to a determined electrical resistance of 18.2 MΩ cm.

UV–visible spectroscopy was obtained using a Shimadzu UV-2450 PC UV–Vis spectrophotometer. Transmission electron microscopic (TEM) image was recorded from a JEM-2010F microscope (Japan). Surface modification was carried out by Fourier transform infrared (FT-IR) spectroscopy (Bruker 70, Germany). Electrochemical characterization was performed using an Autolab PGSTAT128N system (Eco Chemise B.V., The Netherlands). Z-potential and DLS was recordedfrom Malvern Nano Zetasizer (MAL1202556). SPR spectroscopic measurements were performed by a homemade SPR system based on the traditional Kretschmann configuration. A detail schematic diagram of the SPR system and sensor chip configuration was shown in our former work (Chen et al., 2008, 2010). The signal form photodiode was converted through a signal process board (K-MAC Co., Spectra View 2000).

2.2. Sensor surface functionalization

The SPR chip was processed and modified before the experiment. The chip was washed with ethanol and ultrapure water and then cleaned for 30 s using warm piranha solution (30% H_2O_2:H_2SO_4 = 1:3) followed by thorough rinsing with DW and blow-drying with nitrogen. Exactly 200 μL of cDNA solution (including 5 mM TCEP) with a total concentration of 100 nM was prepared and reacted at room temperature for 1 h after complete shaking. The chip was reacted with 100 nM –SH modified complementary DNA solution for over 2 h. After rinsing with DW, the aptamer chip was stored at room temperature prior to the SPR measurements.

2.3. Preparation of GNPs-Apt and MNPs-Ab

Details on the preparation and modification of GNPs-Apt and MNPs-

Ab are provided in the Supporting Information.

2.4. Preparation of MNPs-Ab/BNP/GNPs-Apt and SPR measurement

A total of 50 μL of MNPs-Ab was incubated with BNP for 20 min in a 37 °C metal shaker. The particles were then separated by an external magnet, washed thrice with PBS, and resuspended in 50 μL of PBS. Next, a total of 100 μL of excess GNPs-Apt and MNPs-Ab-BNP was incubated for 30 min in the metal shaker, separated using an external magnet, washed thrice with PBS, and resuspended in 100 μL of PBS to obtain MNPs-Ab/BNP/GNPs-Apt nanocomposites. The nanocomposite was dropped onto the cDNA-coated Au chip for 10 min, after which the unreacted solution was aspirated and washed off with PBS. Finally, SPR angles were measured and collected.

3. Results and discussion

3.1. Experimental principle

As shown in Scheme 1, two types of NPs were used to fabricate the SPR sensor. Previous reports indicate that the Kd values of BNP toward aptamer and anti-BNP are 12.5 and 0.33 nM, respectively, which indicates that the two probes have high individual binding ability to the target BNP (Wang et al., 2015; Tetin et al., 2006). GNPs-Apt and MNPs-Ab can specifically recognize BNP to form magnetoplasmonic nanocomposites for dual screening of the analyte in complex environments. After magnetic separation, the cDNA of Apt immobilized on the Au film is ready to bind with the MNPs-Ab/BNP/GNPs-Apt nanoconjugates in a facile manner through hybridization with the GNPs-Apt. The nanocomposites are formed by cascade conjugation and then modified on the surface of the chip to amplify SPR signals (Scheme 1).

3.2. Characterization of the nanomaterials

Representative TEM images of the GNPs and MNPs are shown in Fig. 1(A) and (D); uniform GNP particles with a diameter of 23.4 nm are observed. The Fe_3O_4 core structure of MNP has a diameter of 275 nm, and the SiO_2 shell with a thickness of 25 ± 2.5 nm is uniformly applied on the surface of Fe_3O_4. These results indicate that the SiO_2 was successfully coated on the surface of the Fe_3O_4 NPs. To analyze the overall morphology of these two NPs, their hydrodynamic behaviors were measured by dynamic light scattering (DLS) (Fig. 1(B) and (E)). A comparatively monodisperse population of GNPs with an average diameter of 21.75 nm, which is reasonable considering the small difference in hydration status and the intensity-based weighting of the DLS data, was observed. However, the average diameter of the DLS data corresponding to the MNPs (Fig. 1(E)) was larger than that observed directly by TEM, which is due to the partial precipitation and uneven dispersion of the MNP solution during the measurement. GNPs before and after BNP aptamer modification were characterized by Fourier transform infrared spectroscopy (ATR-FTIR) (Fig. 1(C)). The modified GNPs showed the characteristic peak of C=O at 1650 cm^{-1}. The stretching vibrations of the N–H bond at 3421 cm^{-1} were not observed in the bare GNPs. These results confirm the presence of the NH_2-aptamer after modification of the thiol group by GNPs. After carboxyl functionalization of the MNPs, specific antibodies were chemically linked to BNP through EDC/NHS activation. The FTIR spectrum of the modified MNPs in Fig. 1(F) reveals peaks related to the N–H bond at 3473 cm^{-1} and C=O bond at 1650 cm^{-1}, which proves the formation of peptide bonds. Peaks of C–H at 2922 cm^{-1} and the C–C bond at 1140–1250 cm^{-1} also indicate successful attachment of the antibody to the MNPs. Finally, the ζ of the unmodified COOH-MNPs in water was measured to be −17.5 mV, while that of the anti-BNP-modified MNPs was −15.1 mV. These results support the successful functionalization of MNPs.

The assembly of GNPs with amino BNP aptamers was observed through UV–vis spectroscopy. As shown in Fig. 2(A), the maximum plasma absorption of the synthesized GNPs appears at 519 nm. The absorption peak at this wavelength corresponds to a typical GNP with an average diameter of 20 ± 3 nm. The absorption peak of the carboxyl-terminated NPs formed by functionalization with MUA is located at 522 nm, and the covalent linkage of COOH-MUA further broadens the absorption band, showing a slight red shift. The final GNPs-Apt colloidal solution showed maximum plasma absorption at 539 nm, thus demonstrating successful modification of the NPs.

Modification of the Au electrode surface was investigated by electrochemical impedance spectroscopy (EIS) to characterize the interaction of cDNA with the MNPs-Ab/BNP/GNPs-Apt nanocomposites (Fig. 2(B)). EIS is a common method used to characterize the electrode surface modification process and has been widely applied to describe various types of molecular assembly on the surface of Au electrodes. Electrochemical impedance data are supplied to an equivalent circuit for quantitative information, and results are usually presented as Nyquist plots. The Randles circuit is used as an equivalent circuit model for impedance data fitting to obtain charge transfer resistance (Sgobbi et al., 2018). In the circuit shown in Fig. 2(B), the impedance of the modified cDNA increased from 153 Ω to 677 Ω, which is attributed to an increase in electron transfer resistance and, in turn, a decrease in electron diffusion capability. This result confirms that the cDNA was

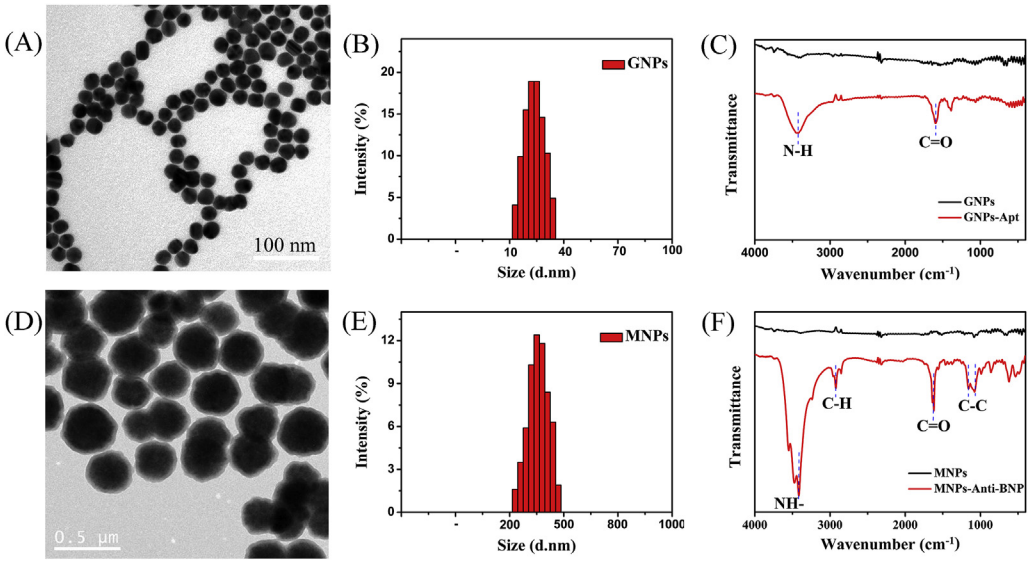

Fig. 1. TEM image (A), DLS data (B), and FTIR spectra (C) before (black) and after (red) aptamer modification of GNPs. TEM image (D), DLS data (E), and (F) FTIR spectra before (black) and after (red) aptamer modification of MNPs. (For interpretation of the references to color in this figure legend, the reader is referred to the Web version of this article.)

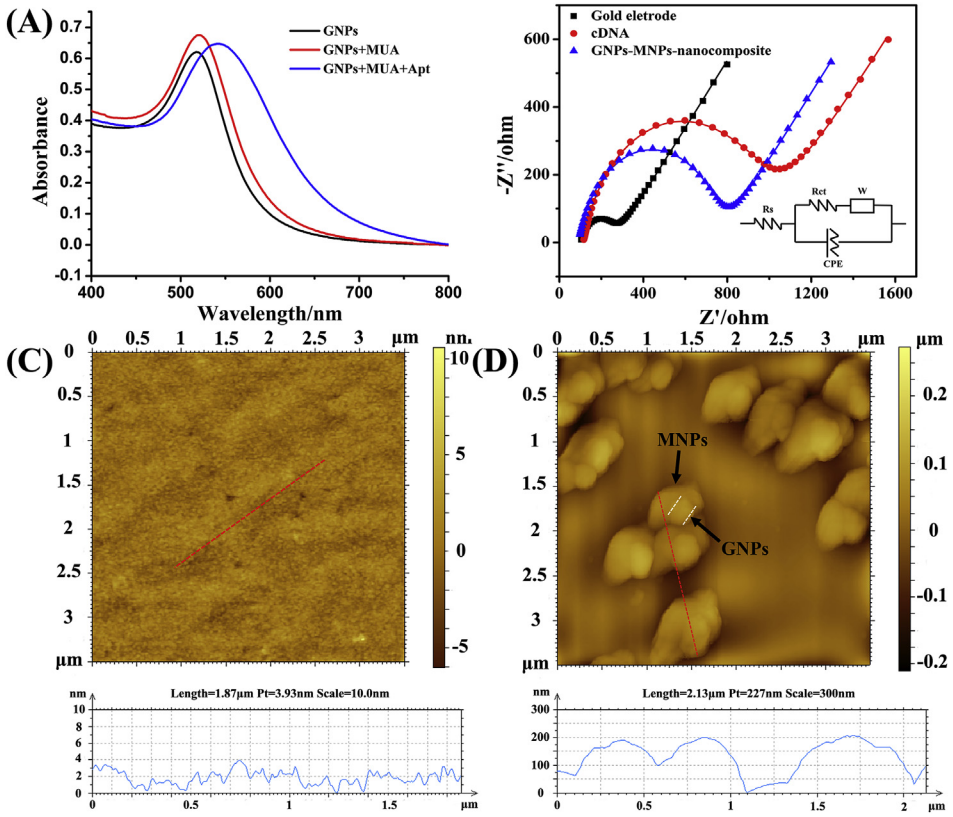

Fig. 2. (A) UV–vis absorption spectra of the process of aptamer modification of GNPs. (B) Electrochemical impedance spectra. Inset: Randles equivalent circuit using a constant phase element. AFM before (C) and after (D) modification of nanocomposites.

successfully immobilized. After incubation of the MNPs-Ab/BNP/GNPs-Apt nanocomposite with the cDNA-modified electrode, the semicircular diameter of the electrochemical impedance of the electrode increased to 814 Ω. The weak conductivity of MNPs contributes to the increase in electron transfer resistance of the electrode. These results indicate that the MNPs-Ab/BNP/GNPs-Apt nanocomposite was attached to the chip surface through hybridization with cDNA.

Atomic force microscopy (AFM) is an ideal tool used to measure particle size distributions and complex arrays of NP because of its superior ability to characterize nanoscale objects. Therefore, AFM was utilized to characterize the surface structure and morphology of the SPR chip surface. Fig. 2(C) and (D) depict 2D images and typical cross-sectional line drawings before and after modification of the nanocomposite, respectively. The corresponding 3D map is shown in Fig. S2. The bare Au chip showed good uniformity, and the relative surface difference was less than 4 nm. The local distribution of interacting MNPs-Ab and GNPs-Apt after hybridization with cDNA is shown in Fig. 2(D). The interconnection of MNPs-Ab and GNPs-Apt by the target BNP reveals the successful formation and attachment of the complex to the surface of the SPR chip.

3.3. Optimization of experimental parameters for BNP detection

We optimized the experimental conditions (Fig. S3), including the pH of the reaction system (Fig. S3(A)), the incubation temperature of the nanocomposite (Fig. S3 (B)), the reaction time with the analyte (Fig. S3(C)), and the concentration of anti-BNP in nanocomposite (Fig. S3(D)). When the incubation temperature was 37 °C in a neutral environment and the modification time was 20 min, the best experimental results were obtained and the reaction was carried out to 94% completion. The concentration of anti-BNP is important for the results of the entire experiment. When the concentration of anti-BNP was 20 μg/mL, the binding process with the target BNP was substantially balanced. Therefore, to achieve the desired experimental results, the following optimal conditions were applied to subsequent experiments: anti-BNP concentration = 20 μg/mL, pH 7, 37 °C, and 20 min.

3.4. BNP detection

Different concentrations of BNP were investigated under optimal experimental conditions to evaluate the performance of two types of NP-based SPR biosensors. The corresponding SPR angles increased proportionally with increasing BNP concentration, as shown in Fig. 3(A). A linear relationship was observed between the SPR angle and the logarithm of the BNP concentration (100 fg/mL to 10 ng/mL). The linear regression equation obtained by fitting was $Y = 217.73 \times \log C\ (pg/mL) + 188.45$, with a correlation coefficient of $R^2 = 0.953$, as depicted in Fig. 3(B). The limit of detection according to three standard deviations of the SPR angle was 28.2 fg/mL. The magnetoplasmonic nanoconjugates promoted strong electric coupling and, in turn, changes in the refractive index of the thin film attached to the chip. The conjugate also changed the actual components of the refractive index with increasing mass of magnetoplasmonic nanoconjugates. These phenomena contribute to the significant sensitivity enhancement of the BNP sensor. The results show that the current strategy has excellent analytical performance and could achieve high sensitivity. The performance of various BNP biosensors was compared with the proposed sensor, and the results are listed in Table S1. The fabricated SPR biosensor showed excellent analytical property for detecting BNP, including a wide linear range and a low detection limit. It is thus capable of detecting BNP in human whole blood early in HF.

3.5. Selectivity of the SPR biosensor

To evaluate the selectivity of the proposed biosensor, the SPR reflectivity curves of a negative control (non-functionalized MNPs and

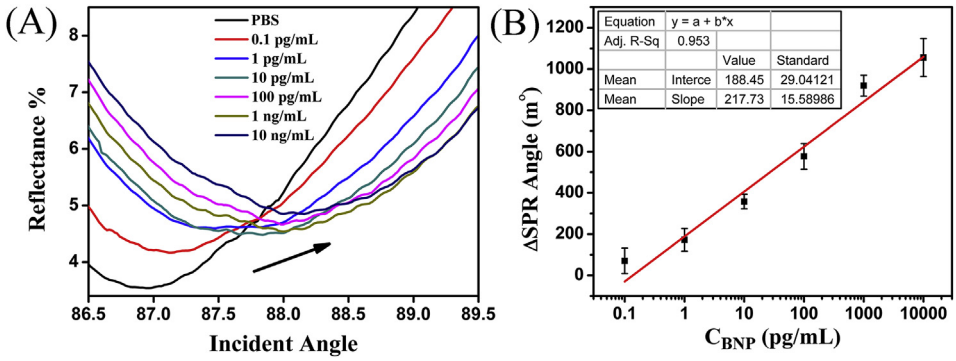

Fig. 3. (A) SPR reflectivity curves during BNP detection at PBS, 0.1 pg/mL, 1 pg/mL, 10 pg/mL, 100 pg/mL, 1 ng/mL, and 10 ng/mL. (B) Linear relationship for BNP determination.

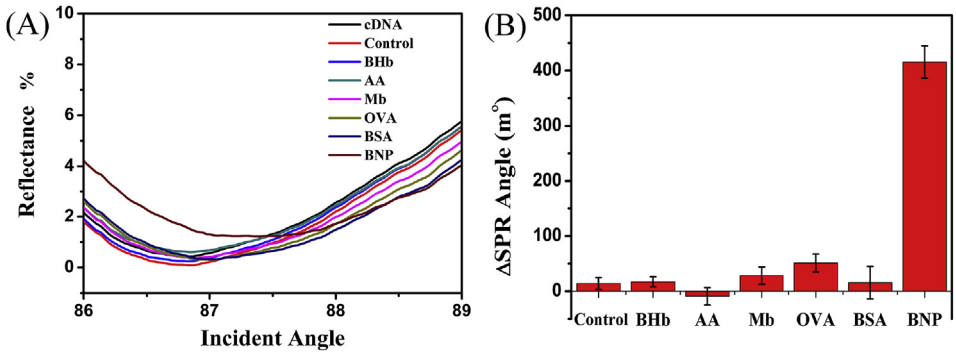

Fig. 4. (A) SPR reflectivity curves and (B) SPR angle shifts during detection of BNP against a negative control and interfering substances.

GNPs) and other proteins that may interfere with BNP detection, including BHb, AA, Mb, OVA, and BSA, were compared as depicted in Fig. 4(A). Fig. 4(B) shows that the sensor's SPR angle shifts toward BNP (100 pg/mL) and different interfering substances (1 ng/mL) under the same conditions. No SPR signal response was observed in the presence of substances other than BNP because specific binding occurs between MNPs-Ab and BNP and cDNA provides dual selective binding to eliminate possible non-specific binding. These outcomes demonstrate that the dual-recognition strategy biosensor has excellent selectivity for determining BNP.

3.6. Serum sample analysis

To investigate the possible applications of the developed SPR sensor in serum samples, serum samples of healthy humans were collected from the First Affiliated Hospital of Zhengzhou University (Zhengzhou, China), and the feasibility of the biosensor for measuring BNP in PBS and serum was tested (Table S2). The relative standard deviations (RSD) of the detection results were less than 6.95%, and the average recoveries in PBS were in the range of 93.5%–103.2%. Assay of serum samples without any form of pretreatment revealed recoveries and RSDs of 92.5%–113.9% and 6.8%–13.8%, respectively (Table 1), thereby indicating the feasibility of the proposed sensor for future clinical measurement. Taken together, the results demonstrate that the method exhibits great accuracy for BNP sensing in real samples and has excellent potential for practical application.

Table 1
Detection and comparison of BNP in clinical serum samples (n = 3).

sample concentration	SPR shifts (m°)	Found (pg/mL)	Recovery %	RSD %
16.93	78.7	15.66	92.5	7.5
53.56	260.3	58.40	109.1	9.0
80.38	331.7	91.54	113.9	13.8
95.23	548.6	101.7	106.8	6.8

4. Conclusions

In summary, a sensitive and dually selective strategy was developed for BNP detection based on analyte-induced NP cascade conjugation. This strategy can be used to analyze BNP at the fg/mL level with excellent specificity and applied to complex biological samples. The performance of the proposed immunosensing system was improved by the combination of MNPs as magnetically separated nanocarriers and GNPs as a connecting medium. The proposed strategy provides great opportunities for determining BNP in biological samples and paves the way for development of valuable analytical tools for clinical HF diagnostics and management.

Declaration of interests

The authors declare that they have no known competing financial interests or personal relationships that could have appeared to influence the work reported in this paper.

The authors declare the following financial interests/personal relationships which may be considered as potential competing interests:

CRediT authorship contribution statement

Jialin Zhao: Conceptualization, Data curation, Formal analysis, Validation, Writing - original draft. **Danli Liang:** Formal analysis, Validation, Writing - original draft. **Shouwei Gao:** Formal analysis, Writing - review & editing. **Xiaojun Hu:** Data curation, Writing - review & editing. **Kwangnak Koh:** Data curation, Writing - review & editing. **Hongxia Chen:** Conceptualization, Project administration, Funding acquisition, Writing - review & editing.

Acknowledgment

This work was supported by the National Natural Science Foundation of China (Grant No. 61275085).

Appendix A. Supplementary data

Supplementary data to this article can be found online at https://doi.org/10.1016/j.bios.2019.111440.

References

Abbas, A., Linman, M.J., Cheng, Q., 2011. Biosens. Bioelectron. 26, 1815–1824.
Ahmed, F.A., Ferial, A.A.M., Abdul-Karim, Y.A.S., 2014 Iraqi. J. Sci. 55, 1541–1546.
Altintas, Z., Fakanya, W.M., Tothill, I.E., 2014. Talanta 128, 177–186.
Babamiri, B., Hallaj, R., Salimi, A., Akhtari, K., 2017. Microchim Acta 184, 3613–3623.
Cao, Y., Griffith, B., Bhomkar, P., Wishart, D.S., McDermott, M.T., 2018. Analyst 143, 289–296.
Chekin, F., Vasilescu, A., Jijie, R., Singh, S.K., Kurungot, S., Iancu, M., Badea, G., Boukherroub, R., Szunerits, S., 2018. Sensor. Actuator. B Chem. 262, 180–187.
Chen, H., Gal, Y.S., Kim, S.H., Choi, H.J., Oh, M.C., Lee, J., Koh, K., 2008. Sensor. Actuator. B Chem. 133, 577–581.
Chen, H., Huang, J., Lee, J., Hwang, S., Koh, K., 2010. Sensor. Actuator. B Chem. 147, 548–553.
Chen, H., Qi, F., Zhou, H., Jia, S., Gao, Y., Koh, K., Yin, Y., 2015. Sensor. Actuator. B Chem. 212, 505–511.
Egesa, D., Chuck, C.J., Plucinski, P., 2018. ACS Sustain. Chem. Eng. 6, 991–999.
Fathi, F., Rashidi, M.-R., Omidi, Y., 2019. Talanta 192, 118–127.
Feng, T., Qiao, X., Wang, H., Sun, Z., Hong, C., 2016. Biosens. Bioelectron. 79, 48–54.
Goetze, J.P., Zois, N.E., 2016. Lancet Diabetes Endocrinol. 4, 840–849.
He, L., Musick, M.D., Nicewarner, S.R., Salinas, F.G., Benkovic, S.J., Natan, M.J., Keating, C.D., 2010. J. Am. Chem. Soc. 122, 9071–9077.
Jain, P.K., Huang, X., El-Sayed, I.H., El-Sayad, M.A., 2007. Plasmonics 2. pp. 107–118.
Jang, H.R., Wark, A.W., Baek, S.H., Chung, B.H., Lee, H.J., 2014. Anal. Chem. 86, 814–819.
Lei, Y.M., Xiao, M.M., Li, Y.T., Xu, L., Zhang, H., Zhang, Z.Y., Zhang, G.J., 2017. Biosens. Bioelectron. 91, 1–7.
Li, S., Yang, M., Zhou, W., Johnston, T.G., Wang, R., Zhu, J., 2015. Appl. Surf. Sci. 355, 570–576.
Li, X., Wei, J., Aifantis, K.E., Fan, Y., Feng, Q., Cui, F.-Z., Watari, F., 2016. J. Biomed. Mater. Res. A 104A, 1285–1296.
Li, H., Hu, X., Zhao, J., Koh, K., Chen, H., 2019a. Electrochem. Commun. 100, 126–133.
Li, X., Liu, L., Dong, X., Zhao, G., Li, Y., Miao, J., Fang, J., Cui, M., Wei, Q., Cao, W., 2019b. Biosens. Bioelectron. 126, 448–454.
Liang, R.P., Yao, G.H., Fan, L.X., Qiu, J.D., 2012. Anal. Chim. Acta 737, 22–28.
Liang, W., Wang, S., Festa, F., Wiktor, P., Wang, W., Magee, M., LaBaer, J., Tao, N., 2014. Anal. Chem. 86, 9860–9865.
Lin, D.C.C., Diamandis, E.P., Januzzi, J.L., Maisel, A., Jaffe, A.S., Clerico, A., 2014. Clin. Chem. 60, 1040–1046.
Liu, R., Wang, X., Aihara, K., Chen, L., 2014. Med. Res. Rev. 34, 455–478.
Liu, Z., Ji, L., Dong, X., Li, Z., Fu, L., Wang, Q., 2015. RSC Adv. 5, 6259–6264.
Lourenço, P., Ribeiro, A., Pintalhão, M., Cunha, F.M., Pereira, J., Marques, P., Vilaça, J.P., Nord, J., Stehlik, Josef, 2009. Am. J. Cardiol. 104, 689–694.
Mei, Q., Ding, X., Chen, Y., Hong, J., Koh, K., Lee, J., Chen, H., 2012. Microchimica Acta 178, 301–307.
Rogers, R.K., Stoddard, G.J., Greene, T., Michaels, A.D., Fernandez, G., Freeman, A., Wang, P., Jin, B., Xing, Y., Cheng, Z., Ge, Y., Zhang, H., Hu, B., Mao, H., Jin, Q., Zhao, J., 2014. J. Nanosci. Nanotechnol., vol. 14, 5662–5668.
Sarangadharan, I., Wang, S.L., Tai, T.Y., Pulikkathodi, A.K., Hsu, C.P., Chiang, H.H.K., Liu, L.Y.M., Wang, Y.L., 2018. Biosens. Bioelectron. 107, 259–265.
Scarano, S., Mascini, M., Turner, A.P.F., Minunni, M., 2010. Biosens. Bioelectron. 25, 957–966.
Serafín, V., Torrente-Rodríguez, R.M., González-Cortés, A., Frutos, P.G., Sabaté, M., Sgobbi, L.F., Machado, S.A.S., 2018. Biosens. Bioelectron. 100, 290–297.
Sgobbi, L.F., Machado, S.A.S., 2018. Biosens. Bioelectron. 100, 290–297.
Tetin, S.Y., Ruan, Q., Saldana, S.C., Pope, M.R., Chen, Y., Wu, H., Pinkus, M.S., Jiang, J., Richardson, P.L., 2006. Biochemistry 45 (47), 14155–14165.
Wang, P., Jin, B., Xing, Y., Cheng, Z., Ge, Y., Zhang, H., Hu, B., Mao, H., Jin, Q., Zhao, J., 2014. J. Nanosci. Nanotechno. 14, 5662–5668.
Wang, J., Munir, A., Zhu, Z., Zhou, H.S., 2010. Anal. Chem. 82, 6782–6789.
Wang, Y., Wu, J., Chen, Y., Xue, F., Teng, J., Cao, J., Lu, C., Chen, W., 2015. Microchimica Acta 182, 331–339.
Wu, B., Jiang, R., Wang, Q., Huang, J., Yang, X., Wang, K., Li, W., Chen, N., Li, Q., 2016. Chem. Commun. 52, 3568–3571.
Xu, R., Lu, P., Wu, B., Wang, X., Pang, X., Du, B., Fan, D., Wei, Q., 2018. Sensor. Actuator. B Chem. 274, 349–355.
Zou, F., Wang, X., Qi, F., Koh, K., Lee, J., Zhou, H., Chen, H., 2017. Sensor. Actuator. B Chem. 250, 356–363.